Coaxial Needle Insertion Assistant With Enhanced Force Feedback

Danilo De Lorenzo*, Yoshihiko Koseki, Elena De Momi, Kiyoyuki Chinzei, *Member, IEEE*, and Allison M. Okamura, *Fellow, IEEE*

***Abstract*—Many medical procedures involving needle insertion into soft tissues, such as anesthesia, biopsy, brachytherapy, and placement of electrodes, are performed without image guidance. In such procedures, haptic detection of changing tissue properties at different depths during needle insertion is important for needle localization and detection of subsurface structures. However, changes in tissue mechanical properties deep inside the tissue are difficult for human operators to sense, because the relatively large friction force between the needle shaft and the surrounding tissue masks the smaller tip forces. A novel robotic coaxial needle insertion assistant, which enhances operator force perception, is presented. This one-degree-of-freedom cable-driven robot provides to the operator a scaled version of the force applied by the needle tip to the tissue, using a novel design and sensors that separate the needle tip force from the shaft friction force. The ability of human operators to use the robot to detect membranes embedded in artificial soft tissue was tested under the conditions of 1) tip force and shaft force feedback, and 2) tip force only feedback. The ratio of successful to unsuccessful membrane detections was significantly higher (up to 50%) when only the needle tip force was provided to the user.**

***Index Terms*—Force feedback, haptics, needle insertion, surgery.**

I. Introduction

In standard manual needle insertions, an operator introduces straight needles into soft tissues of the body for diagnosis (biopsy, blood sampling) and therapy delivery (drug delivery, electrode placement) [1]. In minimally invasive needle insertion, due to the limited access to the surgical site, the surgeon (or other clinician, such as an anaesthesiologist or interventional radiologist) cannot see the path of the needle inside the tissue and thus must rely on a limited sense of touch or an assumed needle path based on correspondence between the amount of insertion and preoperative medical images.

The sense of touch is restricted in that the operator would like to feel the properties of tissues deep within the body, but the interaction with tissue is mediated by the needle. There is no distributed tactile sensation, and force feedback—which includes both tip and shaft forces—is provided only at the base of the needle. Sensing and displaying needle tip forces could allow the surgeon to better estimate the position of the needle inside the tissue [1] and allow more accurate identification of differences in soft tissue resistance (e.g., when hitting a vessel in the brain parenchyma during probe/electrode placement for deep brain stimulation). Improving position accuracy inside the tissue increases the operator's ability to precisely reach the target of the intervention, and identifying differences in tissue properties (e.g., due to contact with subsurface structures such as nerves) could prevent unwanted tissue damage of vital structures along the needle path. This is supported by the results of Gerovich *et al.* [2], who showed in a virtual environment that real-time visual and force feedback improve the ability of users to detect puncture of different tissue layers during needle insertion.

A target application of this research is keyhole neurosurgical interventions, where a straight needle of about 2–3 mm in diameter is inserted from a small opening on the skull to the target inside the brain. In such procedures, vessel rupture (puncture) and subsequent bleeding inside the brain parenchyma is a critical problem of the procedure, with an incidence between 4% and 7% [3]. During the needle advancement, the possibility to detect unexpected situations, like a vessel on the needle trajectory, could prevent this highly dangerous situation, lowering the incidence of hemorrhagic complications inside the brain.

Most robotic devices for minimally invasive surgery and needle insertion do not provide any force feedback; the outer control loop between the operator and the robot relies only on surgeon hand–eye coordination [4], [5]. Whether force feedback improves surgical precision and outcomes in minimally invasive robotic procedures is under debate [6]–[9]; however, some studies confirm that haptic feedback can increase an operator's ability to distinguish between different tissues [10] and reduce tissue damage [11] and surgical task duration [12]. Force feedback to the user is usually achieved with one of the following robot architectures: teleoperation with impedance control, where the user remotely maneuvers the device, or cooperative

Manuscript received March 7, 2012; revised July 3, 2012 and September 21, 2012; accepted October 13, 2012. Date of publication November 16, 2012; date of current version January 16, 2013. This work was supported by the Scuola Interpolitecnica di Dottorato Milano Torino e Bari, the National Institutes of Health under Grant R01 EB006435, the Japan Society for the Promotion of Science under Excellent Young Researcher Overseas Visit Program, The Johns Hopkins University, Advanced Industrial Science and Technology, and the Politecnico di Milano, Italy. *Asterisk indicates corresponding author.*

*D. De Lorenzo is with the Neuroengineering and Medical Robotics Laboratory, Department of Bioengineering, Politecnico di Milano, 20133 Milano, Italy (e-mail: danilo.delorenzo@mail.polimi.it).

Y. Koseki and K. Chinzei are with the Research Institute of Human Life Technology, Advanced Industrial Science and Technology, Tsukuba 305-8568, Japan (e-mail: koseki-y@aist.go.jp; k.chinzei@aist.go.jp).

E. De Momi is with the Neuroengineering and Medical Robotics Laboratory, Department of Bioengineering, Politecnico di Milano, 20133 Milano, Italy, and also with the Consiglio Nazionale delle Ricerche, Istituto di Tecnologie Industriali ed Automazione, 20131 Milano, Italy (e-mail: elena.demomi@polimi.it).

A. M. Okamura is with the Department of Mechanical Engineering, Stanford University, Stanford, CA 94305 USA (e-mail: aokamura@stanford.edu).

Color versions of one or more of the figures in this paper are available online at http://ieeexplore.ieee.org.

Digital Object Identifier 10.1109/TBME.2012.2227316

manipulation, where the user and the robot cooperatively move the surgical instrument (e.g., the needle). Cooperative manipulation, with admittance control and force-to-motion scaling, has demonstrated high accuracy in demanding surgical procedures [13], [14]. A recent comprehensive review of the major minimally invasive surgery robotic systems, with comparisons of their robotic architectures, is provided in [15].

Even though force feedback in teleoperation and cooperative manipulation systems has been an active research area for several decades [5], haptic feedback is still a technical challenge; to date, there exists no commercial robotic assistant device with compelling force feedback to provide information about environment mechanical properties.

In order to sense interaction force between tissue and a surgical instrument, application-specific sensing techniques must be employed [16]. For needle insertion tasks in neurosurgery, small force variations at the needle tip are masked by the relatively large shear friction force between the needle shaft and the surrounding tissue. The design and implementation of force sensors (FSs) for this application are challenging due to the constraints of size, cost, and equipment encumbrance [16]–[18]. The position of the FS on the surgical tool/device plays a significant role. An FS placed at the tip of the instrument allows accurate detection of the interaction forces, but miniaturization, sterilization, insulation, and modification and customization of the standard surgical tool are required. An FS placed far from the instrument tip is not subject to all these requirements, but does not accurately detect the tool–tissue interaction forces, since it integrates mechanical force noise coming from the friction between mechanical interfaces and device inertia [8], [16].

The interaction forces between the needle and the soft tissue, i.e., the friction force along the needle shaft and the pressing/cutting force at the needle tip, were modeled in [19]–[23]. Such models were used in surgical simulators in order to improve the realism of virtual needle insertion for training and planning. Other models [24], [25] were used to improve detection of membrane puncture, by subtracting the modeled friction force from the total force sensed, thus enhancing detection of changes in tip force. Some models [26] take an energetic approach to separate the force contribution during skin piercing. Modeling errors, generated by the inhomogeneous tissue properties and by the force dependence on insertion speed, tissue properties, temperature, and body fluid interaction, can corrupt the tip force estimation.

A different approach is presented by Kataoka *et al.* [27], where an instrumented coaxial needle was proposed to separately measure pressing/cutting force at the needle tip and shear friction on the needle shaft using two different FSs: a one-axis load cell for the needle tip and a six-axis load cell for the shaft force. Similarly, Washio and Chinzei [28] developed a method for robust detection of the instant of puncture, using the tip force information. A tissue model is not needed and the device reliably identifies the two force contributions; its performance is not influenced by modeling errors.

In this paper, we present a robotic assistant based on the coaxial needle scheme, with a cooperative manipulation architecture in which the robot and the surgeon simultaneously drive the surgical needle. Our purpose is to improve operator perception of small variations in tissue properties (e.g., crossing membranes inside the tissue) during needle insertion. FSs, placed far from the needle tip and shaft, allow separate sensing of the shaft and tip forces, so the control algorithm can display only the latter to the operator. The effectiveness of the system was evaluated through an experiment with inexperienced users, who were asked to insert needles into artificial brain tissue and detect the presence of membranes. The device design and preliminary control methods and evaluation were first presented in [29] and [30]. In this study, we changed the control approach, created and analyzed a new system model, and performed a more complete experimental evaluation of the system.

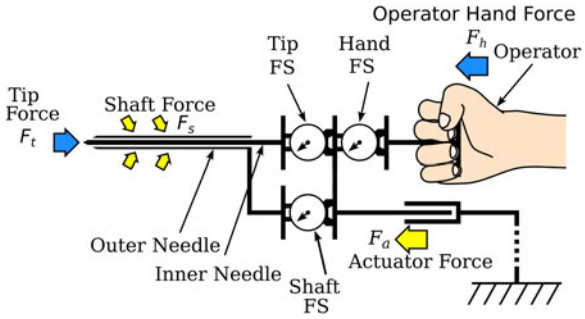

Fig. 1. Overview of the robotic coaxial needle insertion assistant. Three FSs are used to sense the total force applied by the operator (F_h), the force between the outer needle and the tissue (shaft force, F_s), and the force applied by the inner needle to the tissue (tip force, F_t). An actuator drives the motion of the outer and inner needle together with the human operator.

II. Materials and Methods

A. Coaxial Needle Insertion Assistant Design and Control

The device is equipped with a coaxial needle (see Fig. 1), in which an inner needle is inserted into an outer needle. The inner needle tip sticks out of the outer needle; thus, the inner needle is not subjected to friction force due to contact with the surrounding tissue. The two parts of the coaxial needle (inner and outer) are mounted on separate sliders, which are locked together for the implementation presented in this paper, and they move along a linear guide. The inner needle slider is equipped with a handle for the operator to push it. The sliders are driven via a transmission cable by a geared DC motor (Maxon DC Motor, 41.022.022-00.00-202, represented as the actuator in Fig. 1). It has one degree of freedom of linear motion along the needle axis, with 10 mm/s maximum velocity, 10 N maximum force, and 130 mm stroke. Details and a mechanical drawing of the device are provided in [30].

Both the inner and the outer needles are inserted by the operator with the help of the actuator. The device is equipped with four custom-designed FSs sensing the inner needle pressing/cutting (*tip force*, F_t), outer needle (*shaft force*, F_s), operator (*hand force*, F_h), and actuator (F_a) forces, as shown in Fig. 2.

The operator force F_h balances the shaft force F_s, the tip force F_t, and the actuator force F_a. Our system control and analysis assume that the needles do not bend significantly; the needles used are sufficiently stiff such that interaction forces

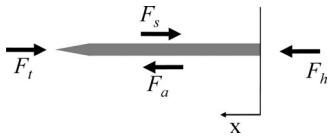

Fig. 2. Forces simultaneously acting on the coaxial needle: F_h is the force exerted by the operator hand, F_t is the force acting on the tip of the needle, F_s is the shaft friction force between the needle and the surrounding tissue, F_a is the actuator force, and x is the positive direction of motion.

between the inner and the outer needles shaft orthogonal to the insertion direction do not affect system performance.

The FS coupled to the inner needle was designed with a full-scale range of 10 N, and the other sensors were designed with a full-scale range of 40 N. The FSs were calibrated with known forces obtained using weights (weight accuracy 20 μN, RMSE = 4.2 mN F_t, 30 mN F_s, 72 mN F_h, 133 mN F_a). Each FS encompasses a flexure parallelogram mechanism with strain gauges connected as a full Wheatstone bridge. Each bridge signal is amplified by instrumentation amplifiers (INA118 and INA128, Texas Instruments). The coaxial needle position is measured by an optical linear encoder (LM-25CPMM-3 S, Encoder Technology, 0.01 mm resolution). The force signals, position signals, and control algorithm are acquired and updated on a computer at 5 kHz with a real-time operating system (RT-Linux/GPL 3.2 rc1 with Linux kernel 2.4.29).

The actuator control scheme shown in Fig. 3 amplifies the forces between the needle and the tissue and displays them to the operator. For this purpose, F_h is proportional to the tissue interaction force measured by the needle sensors (environment force) F_e, through a multiplier ($F_h \cong \alpha F_e$).

F_e can be set by the controller to be equal to the force at the needle tip ($F_e = F_t$) or to the sum of the tip force and the shaft force along the outer needle ($F_e = F_t + F_s$). Fig. 3 shows the two types of force feedback that can be set in the control (*tip* force feedback and *tip+shaft* force feedback).

An outer loop implicit force trajectory-tracking controller [14] was implemented to set the desired needle position (x_d)

$$x_d(t) = k_{if} \int_0^t e_f(t)dt + k_{pf} e_f(t) \tag{1}$$

where $e_f = F_h - \alpha F_e$, and k_{if} and k_{pf} are the integral and proportional outer loop control gains, respectively. The inner loop position control is a proportional controller k_a, which sets the actuator output F_a as

$$F_a = k_a(x_d - x_a) \tag{2}$$

where x_a is the actual position. The position of the actuator x_d is set to minimize the error between the measured and amplified environment force (αF_e) and desired hand forces (F_h), so that the user can feel a scaled version of the needle/tissue interaction forces.

B. Model Analysis

Considering a steady-state (constant velocity) motion, which is usually performed during needle insertion, it is possible to write the force balance equation (see Fig. 2) as

$$F_h = -F_a + F_s + F_t. \tag{3}$$

F_a in (2) can be replaced in (3), resulting in

$$F_h(t) = -k_a(x_d(t) - x_a(t)) + F_s(t) + F_t(t). \tag{4}$$

1) Tip Force Feedback ($F_e = F_t$) Case: Replacing x_d given in (1) and considering $F_e = F_t$, from (4), we obtain

$$F_h = -k_a k_{if} \int_0^t (F_h - \alpha F_t)dt - k_a k_{pf}(F_h - \alpha F_t) + k_a x_a + F_s + F_t \tag{5}$$

which can be rearranged as

$$F_h + k_a k_{pf} F_h - \alpha k_a k_{pf} F_t - F_t = -k_a k_{if} \int_0^t (F_h - \alpha F_t) + k_a x_a + F_s. \tag{6}$$

Considering the simple case where the force feedback on the user hand F_h is not amplified ($\alpha = 1$), it is possible to compute the analytical solution. In a motion with constant velocity (v), $x_a(t) = v \cdot t, F_s$ is proportional (μ = constant) to the depth of the needle inside the tissue x_a as pointed out by Kataoka *et al.* [27]

$$F_s(t) = \mu \cdot x_a(t) = \mu \cdot v \cdot t. \tag{7}$$

With $\alpha = 1$, we can rearrange (6) with respect to the force tracking error $e_f = F_h - F_t$

$$(1 + k_a k_{pf})(F_h - F_t) = -k_a k_{if} \int_0^t (F_h - F_t) + k_a x_a + F_s \tag{8}$$

and we obtain

$$(1 + k_a k_{pf}) e_f = -k_a k_{if} \int_0^t e_f dt + k_a \cdot vt + \mu \cdot vt. \tag{9}$$

The Laplace transform of (9) is

$$(1 + k_a k_{pf}) e_f(s) = -k_a k_{if} \frac{1}{s} \cdot e_f(s) + k_a v \frac{1}{s^2} + \mu v \frac{1}{s^2}. \tag{10}$$

Equation (10) can be rearranged as

$$e_f(s) = \frac{v \cdot k_a}{(1 + k_a k_{pf})s^2 + k_a k_{if} s} + \frac{v \cdot \mu}{(1 + k_a k_{pf})s^2 + k_a k_{if} s}. \tag{11}$$

Computing the inverse transform of (11), we obtain

$$e(t) = \frac{v(\mu + k_a)}{k_a k_{if}} \left[1 - e^{-\frac{k_a k_{if}}{k_a k_{pf} + 1} t}\right] \tag{12}$$

and

$$F_h = \frac{v(\mu + k_a)}{k_a k_{if}} \left[1 - e^{-\frac{k_a k_{if}}{k_a k_{pf} + 1} t}\right] + F_t. \tag{13}$$

Equation (13) shows that the user always feels the tip force plus the contribution of the shaft force (which depends on the insertion velocity v and on the friction coefficient μ) reduced by a factor proportional to the admittance gain k_{if} and k_a in

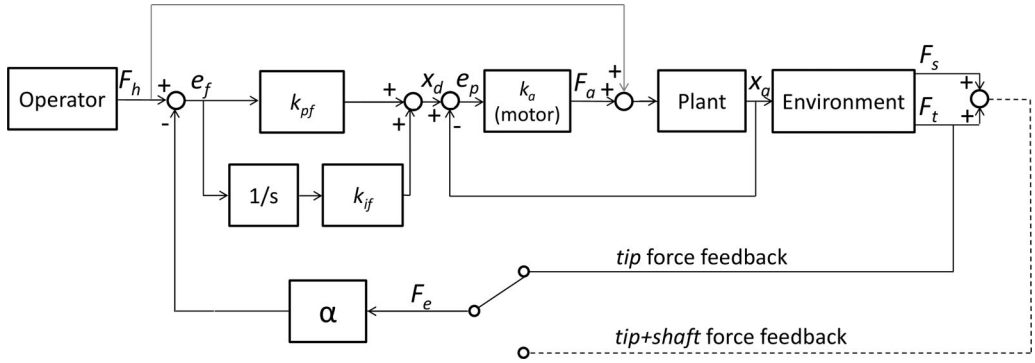

Fig. 3. Coaxial needle control scheme. F_h is the operator hand force, F_e is the needle–tissue interaction force measured by the FSs (F_t and F_s), F_a is the actuator force, k_{if} and k_{pf} are the integral and proportional outer loop control gains, respectively, x_d is the desired position, x_a is the actual position, and e_f is the force tracking error $(F_h - \alpha F_e)$. The two types of force feedback used: *tip* force feedback (solid line), where only the tip force is scaled by a gain α, and fed back to the user; *tip+shaft* force feedback (dotted line), where both the tip F_t and the shaft force F_s are scaled and displayed to the user.

the control loop. This contribution asymptotically reaches the maximum value for $t \to \infty$, where

$$F_h = \frac{v(\mu + k_a)}{k_a k_{if}} + F_t. \tag{14}$$

Thus, even if the force feedback amplification gain is unity ($\alpha = 1$), the user is able to perceive only the tip force plus a scaled contribution of the shaft force. (For $k_a k_{if}$ greater than one, the shaft force contribution is scaled down.) Also, considering the case where velocity is close to zero, the hand force F_h is approximately equal to the tip force, $F_h \approx F_t$. This enables an enhanced perception of the needle–tissue interaction force at the needle tip on the operator hand, substantially reducing the shaft force contribution.

2) Tip+Shaft Force Feedback ($F_e = F_t + F_s$) Case: In the *tip+shaft* force control, (5) can be written as

$$F_h = -k_a k_{if} \int_0^t (F_h - \alpha F_e)dt - k_a k_{pf}(F_h - \alpha F_e) + k_a x_a + F_e. \tag{15}$$

Thus, for $\alpha = 1$

$$(1 + k_a k_{pf})(F_h - F_e) = -k_a k_{if} \int_0^t (F_h - F_e) + k_a x_a \tag{16}$$

and

$$(1 + k_a k_{pf}) e_f = -k_a k_{if} \int_0^t e_f dt + k_a x_a. \tag{17}$$

Applying the Laplace transform, we obtain

$$(1 + k_a k_{pf}) e_f(s) = -k_a k_{if} \frac{1}{s} \cdot e_f(s) + k_a x_a(s) \tag{18}$$

and

$$e_f(s) = \frac{k_a s \cdot x_a(s)}{(1 + k_a k_{pf})s + k_a k_{if}}. \tag{19}$$

When x_a is a *step*, and we take the inverse transform

$$F_h = \frac{k_a}{k_a k_{pf} + 1} \cdot e^{-\frac{k_a k_{if}}{k_a k_{pf}+1} t} + F_e. \tag{20}$$

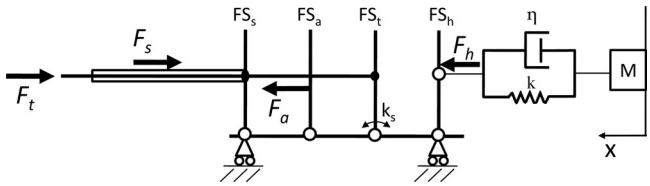

Fig. 4. Hand and device model simulated in the Simscape (Simulink 2011a, Mathworks) environment. F_h is the force exerted by the operator hand, F_t is the force acting only on the tip of the needle, F_s is the shaft friction force between the needle and the surrounding tissue, F_a is the actuator force, and x is the positive direction of motion. FS_s, FS_a, FS_t, and FS_h are the shaft FS, actuator FS, tip FS, and operator hand FS models, respectively. k_s is the elastic constant of the joint spring (sensor elasticity) linking each sensors to the sliding guide. k, η, and M are the elastic constant, the damping coefficient, and the mass of the hand model, respectively [31].

The operator hand force is exactly equal to the environment force for $t \to \infty$ ($F_h = F_e$). When x_a is a *ramp*, $x_a(t) = v \cdot t$

$$F_h = \frac{v}{k_{if}} \left[1 - e^{-\frac{k_a k_{if}}{k_a k_{pf}+1} t}\right] + F_e. \tag{21}$$

Here, for $t \to \infty$, F_h is equal to F_e plus a force contribution that depends on the slope v of the position *ramp* and which is scaled by k_{if}.

C. Simulations

In order to analyze the system force tracking performance as a function of the variation of the force feedback amplification gain α, we simulated the robotic coaxial needle insertion assistant system using Simscape (Simulink 2011a, Mathworks), as shown in Fig. 4.

Each FS was modeled as a beam with one angular degree of freedom. The beam is attached to a carriage with a spring, which models the elasticity of the beam itself.

The applied tip force (F_t, Fig. 5) was set to an initial constant force [0–15 s], then to an increasing ramp [15–27 s] with a quick drop to zero (which simulates the membrane rupture). The shaft force F_s was modeled as a force constantly increasing with time (see Fig. 5). These tip and shaft force profiles were chosen according to experimental evidence (see Section III-B) and the work of Kataoka *et al.* [27]. The desired hand position

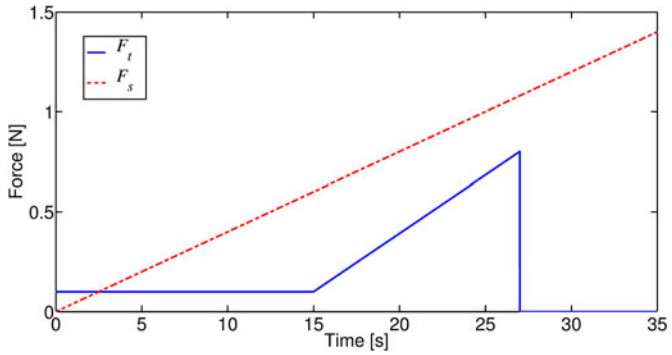

Fig. 5. Simulated shaft force F_s and tip force F_t applied on the inner needle and outer needle, respectively.

was given as an input to the model and was assumed to proceed with constant velocity. In our experiments (described in the following section), operators inserted needles with nearly constant velocity or with repeated nearly constant velocity movements. The actuator force F_a is then the output of the control loop, as shown in Fig. 3. The hand was assumed to be a simplified mass–spring–damper model with parameters derived from [31].

In the simulations, the force feedback amplification gain α was varied from 1 to 9 and the admittance gains k_{if} and k_{ip} were empirically set equal to 200 mm/N and 300 mm/N·s, as a tradeoff between force tracking performance and stability of the control.

D. Experiment Design

In order to test the system performance in detecting brain vessels, six samples of polyvinyl chloride (PVC) rubber mimicking brain soft tissue were prepared. Two membranes made of silicone material (Smooth-on 910) with 0.4- and 0.8-mm thickness, roughly resembling brain vessel walls, were placed inside the artificial soft tissue at three different depths: 15, 35, and 55 mm. The samples were prepared keeping the same compliance ratio between the brain parenchyma and the vessel walls. For brain parenchyma, we used data from [32], while for the vessel walls, we considered the work of Monson *et al.* [33]. Young's modulus for the silicone membranes and PVC rubber brain-mimicking material were 0.66 MPa and 4 kPa, respectively. The resulting ratio between brain and vessel stiffness was 0.006. A steel coaxial needle designed for biopsy was used. The hollow needle outer diameter is 2 mm and the wall thickness of the needle is 0.15 mm. The inner needle diameter is 1.7 mm.

Eleven right-handed, neurologically healthy users participated in this study, which was approved by the Johns Hopkins University Homewood Institutional Review Board. The users were seated, holding the handle of the needle with the right hand. The distance between the tip of the inner needle and the beginning of the outer shaft was set to 5 mm. The tissue was covered except for the entry point of the needles so that the users could not visually discern the position of the membrane inside the samples (see Fig. 6). In each trial, one of the two force feedback conditions was randomly applied to the user hand:

1) the tip force (*tip* force feedback);
2) tip and shaft force (*tip+shaft* force feedback);

with the following pseudorandomly varying conditions:

1) two membrane thicknesses (0.4 and 0.8 mm);
2) three membrane depths (15, 35, and 55 mm);
3) three different amplifications of feedback ($\alpha = 3, 6, 9$).

The insertion order for all these parameters was randomly changed among users. The users were blinded to all the varying conditions (membrane depth and thickness, feedback amplification, type of feedback). Each user performed 15 min of practice to understand the device behavior. During the experiment, the number of insertions performed by each user was 36 and the total number of insertions performed by all users was 396.

Users were asked to blindly insert the biopsy needle into the sample and press a button as soon as they perceived a membrane [see Fig. 7(a)]. The time at which the button was pressed was recorded together with tip position and force data throughout the insertion. The users were then asked to continue inserting the needle until they perceived a membrane puncture, and to stop advancing the needle immediately after the puncture occurred. The insertion was considered "successful" only if the user pressed the button within a time window that starts at the time the needle touches the membrane and ends immediately before the puncture occurs [see Fig. 7(a), after C and right before E]. The insertion was considered "unsuccessful" if the user pressed the button before the needle touched the membrane, if the user pressed the button after having punctured the membrane, or if the button was not pressed.

After having conducted a multivariate analysis, the success rates (number of successful events divided by the total number of trials) of membrane detection prior to puncture using the two types of force feedback (*tip* force feedback and the *tip+shaft* force feedback) were compared with a Wilcoxon test ($p < 0.05$).

Successful insertion performances of the two force feedback conditions were compared combining different thicknesses and force amplification gains (α) (Wilcoxon and Chi-square tests, $p < 0.05$).

Whenever the user pressed the button prior to reaching the membrane, a "false positive detection" was identified, while an "overshoot" was identified when the user pressed the button after the membrane puncture. The false positive ratio and the overshoot ratio with respect to the membrane depth using the two force feedback conditions were compared (Wilcoxon test, $p < 0.05$).

Also, the time to reach the membrane was computed as the time between the needle's first contact with the tissue [point A in Fig. 7(b) and (c)] sample and the time of first contact with the membrane [point C in Fig. 7(b) and (c)]. We used a Wilcoxon test ($p < 0.05$) to compare the time to reach the membrane, with respect to the depth of the membrane, under the two force feedback conditions.

We also measured the average velocity while the needle pressed on the membrane prior to puncture, and examined whether this "pressing velocity" was correlated with insertion success. The average pressing velocity ($\bar{v}$) was computed as the ratio of the traveled distance between the time of first contact with the membrane [point C in Fig. 7(b) and (c)] and the time

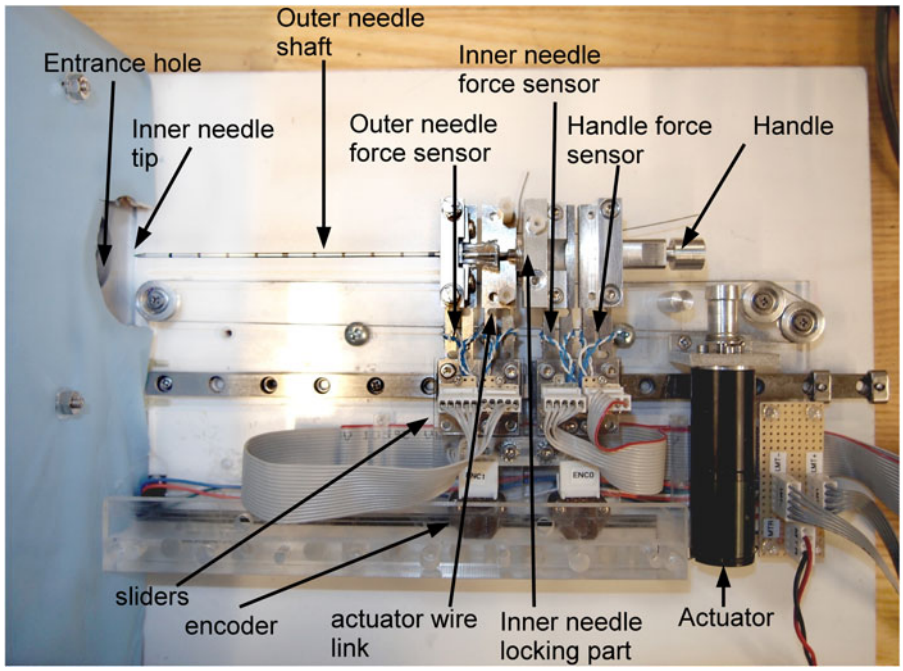

Fig. 6. Coaxial needle testing experimental setup. The blue sheet on the left is covering the tissue sample leaving only the entry point visible to the user.

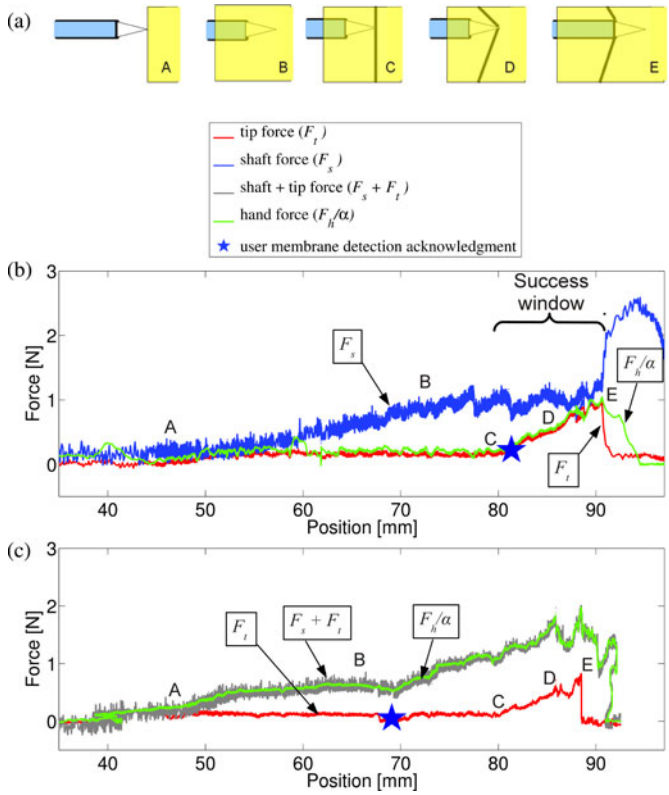

Fig. 7. (a) Phases and events of the needle insertion: free motion in air (A), surrounding tissue entering (B), membrane touching (C and D), and puncture (E). During user experiments, subjects were asked to press a button as soon as they perceived contact with a membrane (between C and D), and stop moving the needle as soon as they detected that puncture had occurred (E). (b) Example of signals for a successful insertion with *tip* force feedback: the user detects the presence of the membrane before the puncture (star). (c) Example of signals for an unsuccessful insertion with *tip+shaft* force feedback: the user detects the presence of the membrane before reaching the membrane (star).

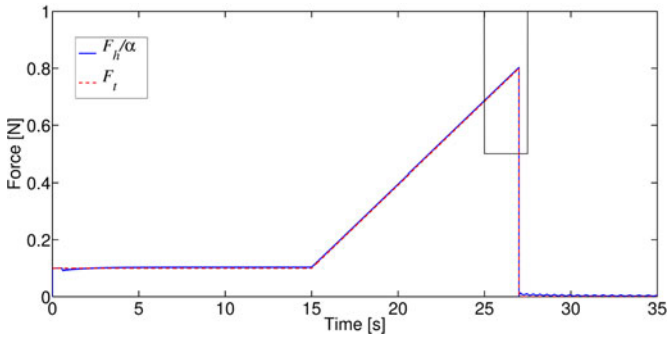

Fig. 8. Simulation results for $\alpha = 9$. Operator hand force (solid line) is already scaled by α in order to be superimposed to the tip force (dashed line). The black box is the signal window shown in Fig. 9.

just prior to puncture [point E in Fig. 7(b) and (c)] and the time needed to travel the distance, i.e.,

$$\bar{v} = \frac{p(E) - p(C)}{t(E) - t(C)} \tag{22}$$

where p is the position of the needle and t is the time. Since the data were normally distributed, we computed the mean and the standard deviation of the velocities for successful and unsuccessful insertions, and compared them with respect to the depth of the membrane, under the two force feedback conditions (T test, $p < 0.5$). All the statistical tests were performed using MATLAB R2011a software (Natick, MA).

III. Results

A. Simulation Results

Simulation results showed that the operator hand force F_h follows the shape of the tip force F_t (see Fig. 8). Increasing

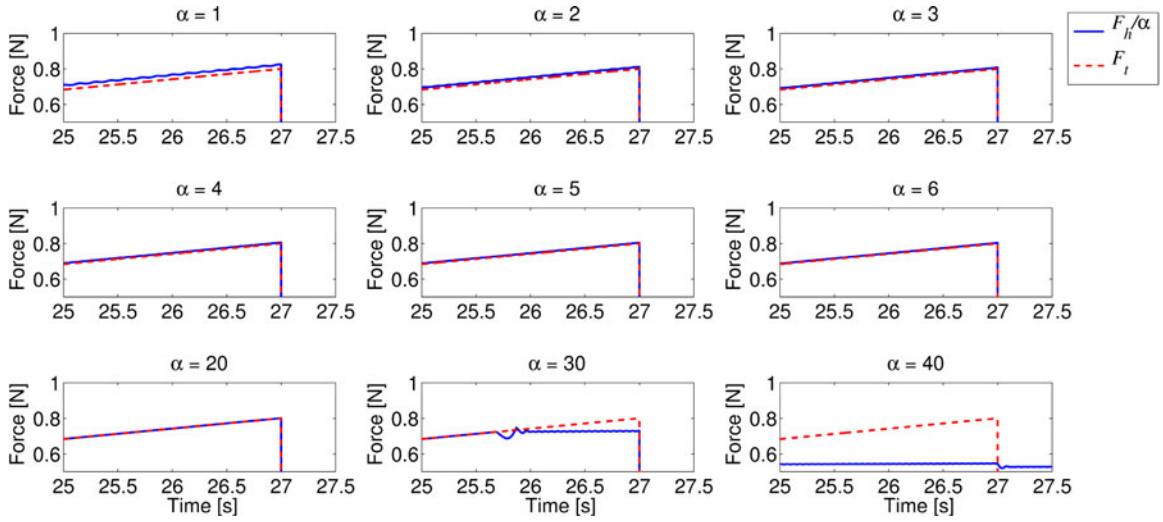

Fig. 9. Simulation results with varying $\alpha = 1,\ldots, 40$ from left to right and from top to bottom. The operator hand force F_h (thick line) is scaled again by α in order to be superimposed to the tip force (F_t, dashed line). These graphs are the zoomed view of Fig. 8 in the interval time [25–27.5 s].

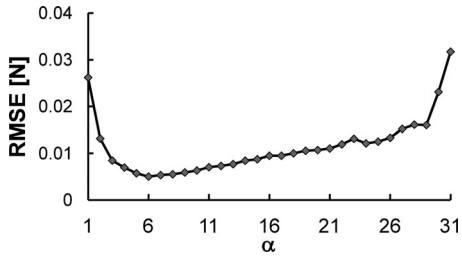

Fig. 10. RMSE between F_h and F_t with α (tip force scaling gain) increasing from 1 to 31, based on a simulation with *tip* force feedback modality. The simulated signals used as force inputs are shown in Fig. 5 and the corresponding simulation results are shown in Figs. 8 and 9. See the text for explanation on the simulation environment.

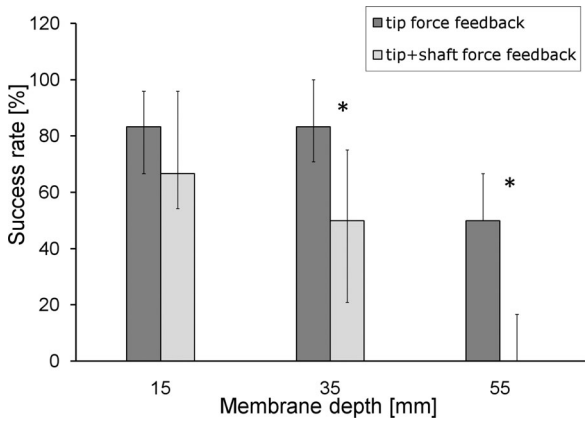

Fig. 11. Median success rate (see the text for the explanation of the term) in membrane detection with respect to membrane depth and feedback type (*tip* force or *tip+shaft* force feedback). The star indicates statistical significance (p values: 0.71, 0.0031, and 0.0014), and the bars indicate the 25th and 75th percentiles. (In some cases, the percentile is coincident with the median.)

the force feedback amplification gain α results in reduction of the force tracking error ($e_f = F_h - \alpha F_t$) (see Fig. 9) and the small oscillations visible in the top left panel of Fig. 9 ($\alpha = 1$), for values of α less than 6. Fig. 10 shows the root mean square error (RMSE) between the scaled F_h and F_t for $\alpha = 1,\ldots, 40$. The RMSE of force tracking initially decreases with increasing α, but then starts to grow again after $\alpha = 6$. Starting from $\alpha = 29$, the RMSE rapidly increases and the system becomes unstable. The same analysis was performed with the *tip+shaft* force feedback. For this scenario, the RMSE starts to grow with α greater than 7 and the system becomes unstable for $\alpha > 12$. Changing the user hand model parameters or the FS stiffness would change the value of α at which the system could become unstable.

B. Experimental Results

Fig. 7(b) shows the tip force F_t, shaft force F_s, and hand force F_h profiles, divided by the force gain α. The tip force is almost constant when the needle is advancing in the artificial tissue (from 45 to 80 mm); then, F_t increases when the needle touches the membrane (point B). Then, the tip force drops rapidly after membrane puncture occurs (at 90 mm). The shaft force F_s gradually increases until the tip of the needle reaches the membrane (C). After that point, the tip force rapidly increases, while the shaft force is almost constant. Immediately after the membrane puncture, the shaft force rapidly increases because the membrane meets the outer needle and starts pushing it. After the user stops, the hand F_h and cutting force F_t go to zero, while F_s decreases to its value prior to contact with the membrane.

Fig. 11 summarizes the performance of users with the two force feedback conditions in terms of success rate of membrane detection with respect to membrane depth. The success rate is always greater when only the *tip* force is provided to the user (median 83.3% versus 66.6% in the case of the 15-mm membrane depth, 83.3% versus 50% for 35-mm depth, and 50% versus 0% for 55-mm depth, Wilcoxon p values: 0.71, 0.0031, 0.0014). For the *tip+shaft* force feedback, performance decreases with the depth of the membrane.

Fig. 12 shows detailed data for success rate in membrane detection with respect to both membrane depth and the various amplification gains. The performance of *tip* force feedback is

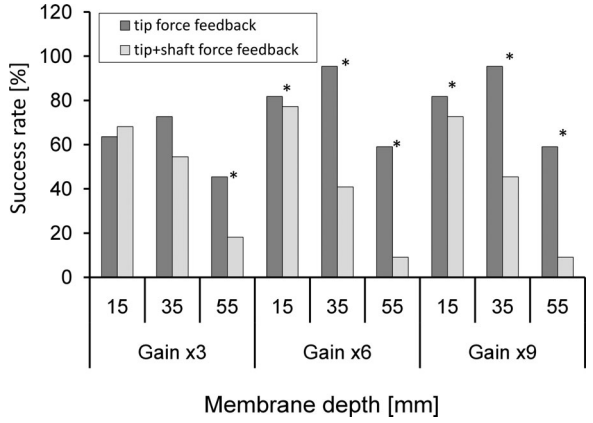

Fig. 12. Success rate in membrane detection with respect to membrane depth (15, 35, and 55 mm) and with different force amplification gains ($\alpha = 3, 6, 9$) in the two force feedback cases (*tip* force or *tip+shaft* force feedback). The star indicates statistical significance (p values: 0.13, 0.12, 0.033; 0.0054, 0.0021, 0.0054; 0.0095, 0.0024, and 0.0054).

TABLE I
FALSE POSITIVES [%] FOR MEDIAN AND 5TH AND 95TH PERCENTILES

	15 [mm]			35 [mm]			55 [mm]		
	Median	5th	95th	Median	5th	95th	Median	5th	95th
tip force	0	0	16	0	0	0	0	0	33
tip+shaft force	0	0	17	33	0	99	83	0	100

TABLE II
OVERSHOOTS [%] FOR MEDIAN AND 5TH AND 95TH PERCENTILES

	15 [mm]			35 [mm]			55 [mm]		
	Median	5th	95th	Median	5th	95th	Median	5th	95th
tip force	0	0	67	0	0	49	0	0	50
tip+shaft force	17	0	50	0	0	33	0	0	0

significantly better than *tip+shaft* force feedback (Chi-square $p < 0.033$, see Fig. 12 for details) for high gains, but not for lower gains.

No statistical difference was found for the success rate with respect to the membrane thicknesses (Wilcoxon, p value $=$ 0.1343).

Table I shows the false positive ratio with respect to the membrane depth for both the force feedback types (*tip* and *tip+shaft*). In the case of *tip* force feedback, the false positive ratio median value is 0% for deep membranes, while in the case of *tip+shaft* feedback, the ratio median value is 83% for deep membranes. In Table I and later data analysis, median values and percentiles are used to present non-normally distributed group data.

Table II shows the overshoot ratio with respect to the membrane depth for both force feedback types. The number of overshoots is close to zero median value among all the considered conditions, except for the *tip+shaft* case, where the median value is 17% for the 15-mm membrane depth.

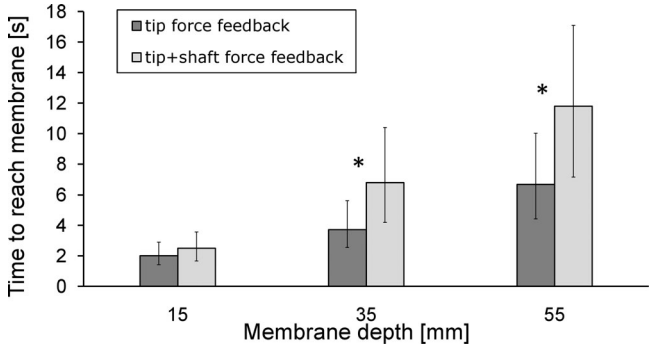

Fig. 13. Median values of time to reach membrane (see the text for the explanation of the term) with respect to membrane depth and feedback type (*tip* force or *tip+shaft* force feedback). The star indicates statistical significance (p values: 0.17, 2.02×10^{-6}, and 5.95×10^{-6}), and the bars indicate the 25th and 75th percentiles.

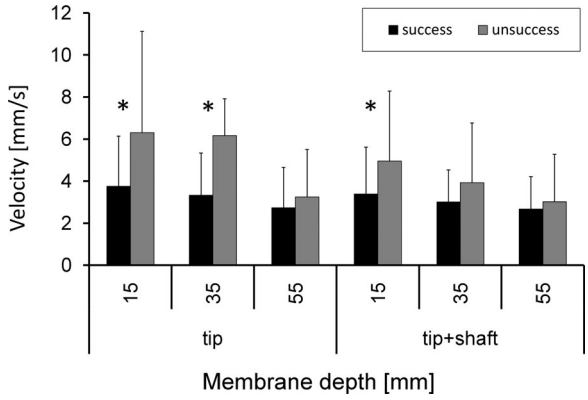

Fig. 14. Mean velocity values with respect to membrane depth (15, 35, and 55 mm) in the two force feedback cases (*tip* force or *tip+shaft* force feedback) for successful and unsuccessful trials. The star indicates statistical significance (p values: 0.0092, 0.0004, 0.3300, 0.0395, 0.1544, and 0.6742) and the bars indicate the standard deviation.

The median value of the time to reach the membrane (see Fig. 13) increases with the depth of the membrane as expected, but with a lower variation (i.e., higher insertion speed) for the *tip* force feedback (Wilcoxon p values: 0.17, 2.02×10^{-6}, 5.95×10^{-6}). Also, the time difference between the two force feedback types increases with the depth of the membrane.

The value of the mean pressing velocity (see Fig. 14) in the case of successful insertions is significantly lower than in the case of unsuccessful insertions for three experimental conditions: *tip* force feedback with 15- and 35-mm membrane depth and for *tip+shaft* force feedback with 15-mm membrane depth (*t*-test, see Fig. 14).

IV. DISCUSSION

The results analytically and experimentally show that the coaxial needle assistant facilitates the perception of membranes during the needle insertion when an amplified version of the force at the needle tip is provided to the user. Even with coaxial needles, if the tip force is not amplified, membrane detection is difficult, due to the small amplitude of tip forces compared to total forces. In the model analysis, we showed the efficacy

of the control in removing the shaft force contribution even without the force amplification gain ($\alpha = 1$). Simulation results showed that increasing the force amplification gain allows better tip force trajectory tracking and reduces small oscillations due to the intrinsic compliance of the force-sensing elements. Increasing the feedback amplification gain above $\alpha = 6$ does not improve the tracking error, but worsens it. The simulation does not consider the interaction force between the inner and the outer needle and the interfering forces acting perpendicular to the needle shaft. This can be further investigated, since in the case of very thin needles, perpendicular forces can bend the needle and increase the friction force between the inner and the outer needle, thus lowering the quality of the force signal. Also, no soft tissue model was used, since we directly applied the tip and shaft force profiles. A further analysis could include a viscoelastic soft tissue model [34].

Experimental results showed that the *tip* force feedback method results in better performance than providing the overall interaction forces between the needle and the tissue (tip and shaft forces together). This is an intuitive result, considering Weber's Law of perception, which states that the ratio of the increment threshold to the background intensity is constant. In the case of large background loads, small force variations are not felt by the human operator. As expected, the gap in performance between the *tip* force feedback and the *tip*+*shaft* force feedback increases with membrane depth inside the surrounding tissue; the larger the depth, the larger the shaft force that masks the small force variations at the needle tip. In the case of the membrane placed at the shallowest depth (15 mm), the shaft force is not large enough to mask the tip force. Thus, it is not surprising that there is no evidence of a difference between the two force feedback approaches at this depth.

Increasing the force feedback gain significantly improves the performance of the *tip* force feedback with respect to the *tip*+*shaft* force feedback, especially for larger membrane depth (35 and 55 mm).

The *tip* force feedback significantly decreases false positive detection. We desire the number of false positives to be as small as possible since false positives increase the procedure duration in clinical practice, due to the need for repeated checking with other types of detection modalities (e.g., medical imaging).

Overshoots represent a small number of failures with respect to false positive detection for all the different experimental conditions. Certain users seemed to take a conservative approach, where the acknowledgment of a false positive detection is preferred to overshoot and puncture of the membrane. For the *tip*+*shaft* force feedback, the median value is zero for the 35 and 55 mm membrane depths, while it is 17% for the 15 mm depth. It is possible that the friction force helps the user to prevent overshoot, thus increasing the number of false positives at larger depths in comparison to the shallowest depth.

With the *tip* force feedback, we found shorter insertion time (i.e., time to reach the membrane) with the *tip*+*shaft* approach. With this force feedback condition, users moved more confidently and quickly with better feedback. We did not consider the response time between the user perception of the membrane and the pressing of the button on the keyboard. Since this condition was the same in both the force feedback conditions, this did not affect comparison between the conditions. No learning curve was found, i.e., for all users, the time to reach the membrane did not increase or decrease with insertion number.

We found a relationship between the membrane pressing velocity and the success of membrane detection for lower membrane depth. Successful membrane identifications correspond to lower pressing velocities. This happened for two of the three membrane depths for the *tip* force feedback, but only with the lowest membrane depth for the *tip*+*shaft* force feedback.

The experiments were performed using samples of brain and vessel mimicking material; artificial tissues are necessary for repeatability of the stimulus between users. The difference in tissue compliance for the brain with respect to the vessels was derived from the literature. Matching needle–tissue friction properties and fracture mechanics properties of the artificial tissues to real brain tissue would increase the relevance of our experiment, but such data for brain tissue are not currently available. However, the range of values for the interaction forces between the needle and the artificial tissue [see Fig. 7(b)] is close to those found in the literature for *ex vivo* needle insertion into swine brain parenchyma [35], [36].

In the experiments, we tested performance with different resistance to puncturing (two different wall thicknesses). The behavior in these two conditions was the same. The analysis of system performance on more membrane thicknesses is of interest and can be further evaluated in future human subject experiments.

The remote configuration of the sensors, which are not positioned directly on the needle, allows detection of interaction forces with standard needles already used for biopsy. With this configuration, the needles are quickly and easily replaced. However, friction between the inner and outer needles can degrade haptic feedback to the user, especially for high force gain, since the user feels not only the cutting force at the tip of the needle, but also the friction force from the outer needle moving relative to the inner needle. In the experimental trials, cleaning the needle between each user experimental session solved the problem. Also, friction is correlated with misalignment between the outer needle and the inner one. Attention was paid in the apparatus design in order to ensure needle alignment.

V. Conclusion and Future Work

In this paper, we propose a robotic coaxial needle assistant equipped with FSs that allows a user to detect the interaction force between a needle tip and surrounding soft tissue, thus enhancing the perception of tissue mechanical property changes during needle advancement. The paradigmatic application is keyhole neurosurgery, in which needles are inserted into the brain parenchyma for biopsy, drug release, or electrode placement. With a conventional needle, soft membranes are generally not detectable because high friction forces mask the small changes in force occurring upon membrane contact. In our approach, the user perceives only the contact force between the

tip of the needle and the tissue, without feeling the increasing friction force along the shaft during the insertion. In comparison with telemanipulation, the proposed cooperative manipulation control scheme allows the user to manipulate the same instrument that is performing the surgery, and still permits force-to-motion scaling [14].

In this study, we demonstrated effectiveness of the coaxial needle insertion assistant, providing *tip only* force feedback enhanced user membrane detection during needle insertion, in comparison to *tip+shaft* force feedback. The ability of our system to provide to the user only the tip force could help the operator in many procedures involving needle insertion, where the detection of membranes or different type of tissues can improve the performance or the success of the intervention.

The capability of our device to separate tip and shaft force contributions during needle insertions into *in vivo* biological tissues must be carefully tested to evaluate clinical relevance and to acquire data for soft tissue model identification. In addition, previous studies showed that the role of haptic feedback could be different for experienced and inexperienced surgeons [2], [4], so the role of tip-force enhancement should be tested for novice and expert clinicians.

REFERENCES

[1] N. Abolhassani, R. Patel, and M. Moallem, "Needle insertion into soft tissue: A survey," *Med. Eng. Phys.*, vol. 29, no. 4, pp. 413–431, 2007.

[2] O. Gerovich, P. Marayong, and A. M. Okamura, "The effect of visual and haptic feedback on computer-assisted needle insertion," *Comput. Aided Surg.*, vol. 9, pp. 243–249, 2004.

[3] R. Grossman, S. Sadetzki, R. Spiegelmann, and Z. Ram, "Haemorrhagic complications and the incidence of asymptomatic bleeding associated with stereotactic brain biopsies," *Acta Neurochir. (Wien)*, vol. 147, no. 6, pp. 627–631, Jun. 2005.

[4] P. Mozer, A. W. Partin, and D. Stoianovici, "Robotic image-guided needle interventions of the prostate," *Rev. Urol.*, vol. 11, pp. 7–15, 2009.

[5] A. M. Okamura, "Haptic feedback in robot-assisted minimally invasive surgery," *Curr. Opin. Urol.*, vol. 19, no. 1, pp. 102–107, Jan. 2009.

[6] C. R. Wagner and R. D. Howe, "Force feedback benefit depends on experience in multiple degree of freedom robotic surgery task," *IEEE Trans. Robot.*, vol. 23, no. 6, pp. 1235–1240, Dec. 2007.

[7] M. Zhou, J. Perreault, S. D. Schwaitzberg, and C. G. L. Cao, "Effects of experience on force perception threshold in minimally invasive surgery," *Surg. Endosc.*, vol. 22, no. 2, pp. 510–515, Feb. 2008.

[8] G. Hager, A. Okamura, P. Kazanzides, L. Whitcomb, G. Fichtinger, and R. Taylor, "Surgical and interventional robotics: part III [Tutorial]," *IEEE Robot. Autom. Mag.*, vol. 15, no. 4, pp. 84–93, Dec. 2008.

[9] M. Zhou, D. B. Jones, S. D. Schwaitzberg, and C. G. L. Cao, "Role of haptic feedback and cognitive load in surgical skill acquisition," in *Proc. 51st Annu. Meet. Human Factors Ergon. Soc.*, 2007, pp. 631–635.

[10] G. Tholey, J. P. Desai, and A. E. Castellanos, "Force feedback plays a significant role in minimally invasive surgery: Results and analysis," *Ann. Surg.*, vol. 241, no. 1, pp. 102–109, Jan. 2005.

[11] C. R. Wagner, N. Stylopoulos, P. G. Jackson, and R. D. Howe, "The benefit of force feedback in surgery: Examination of blunt dissection," *Presence Teleoperators Virtual Environ.*, vol. 16, no. 3, pp. 252–262, Jun. 2007.

[12] C. G. L. Cao, M. Zhou, D. B. Jones, and S. D. Schwaitzberg, "Can surgeons think and operate with haptics at the same time?" *J. Gastrointest. Surg.*, vol. 11, no. 11, pp. 1564–1569, Oct. 2007.

[13] J. Roy, D. L. Rothbaum, and L. L. Whitcomb, "Haptic feedback augmentation through position based adaptive force scaling: Theory and experiment," in *Proc. IEEE/RSJ Int. Conf. Intell. Robots Syst.*, 2002, pp. 2911–2919.

[14] J. Roy and L. L. Whitcomb, "Adaptive force control of position/velocity controlled robots: Theory and experiment," *IEEE Trans. Robot. Autom.*, vol. 18, no. 2, pp. 121–137, Apr. 2002.

[15] G. Dogangil, B. L. Davies, and F. Rodriguez y Baena, "A review of medical robotics for minimally invasive soft tissue surgery," in *Proc. Inst. Mech. Eng. H, J. Eng. Med.*, 2010, vol. 224, no. 5, pp. 653–679.

[16] P. Puangmali, K. Althoefer, L. D. Seneviratne, D. Murphy, and P. Dasgupta, "State-of-the-art in force and tactile sensing for minimally invasive surgery," *IEEE Sens. J.*, vol. 8, no. 4, pp. 371–381, Apr. 2008.

[17] A. L. Trejos, R. V. Patel, and M. D. Naish, "Force sensing and its application in minimally invasive surgery and therapy: A survey," *Proc. Inst. Mech. Eng. C, J. Mech. Eng. Sci.*, vol. 224, no. 7, pp. 1435–1454, Jan. 2010.

[18] D. De Lorenzo, E. De Momi, I. Dyagilev, R. Manganelli, A. Formaglio, D. Prattichizzo, M. Shoham, and G. Ferrigno, "Force feedback in a piezoelectric linear actuator for neurosurgery," *Int. J. Med. Rob. Comput. Assisted Surg.*, vol. 7, pp. 268–275, 2011.

[19] S. P. DiMaio and S. E. Salcudean, "Needle insertion modeling and simulation," *IEEE Trans. Robot. Autom.*, vol. 19, no. 5, pp. 864–875, Oct. 2003.

[20] L. Barbé, B. Bayle, M. de Mathelin, and A. Gangi, "Needle insertions modeling: Identifiability and limitations," *Biomed. Signal Process. Control*, vol. 2, no. 3, pp. 191–198, Jul. 2007.

[21] A. Asadian, R. V. Patel, and M. R. Kermani, "A distributed model for needle-tissue friction in percutaneous interventions," in *Proc. IEEE Int. Conf. Robot. Autom.*, May 2011, pp. 1896–1901.

[22] A. Carra and J. C. Avila-Vilchis, "Needle insertion modeling through several tissue layers," in *Proc. 2nd Int. Asia Conf. Inf. Control, Autom. Robot.*, 2010, pp. 237–240.

[23] R. Kikuuwe, Y. Kobayashi, and H. Fujimoto, "Coulomb-friction-based needle insertion/withdrawal model and its discrete-time implementation," in *Proc. EuroHaptics*, 2006, pp. 207–212.

[24] A. M. Okamura, C. Simone, and M. D. O'Leary, "Force modeling for needle insertion into soft tissue," *IEEE Trans. Biomed. Eng.*, vol. 51, no. 10, pp. 1707–1716, Oct. 2004.

[25] L. Barbe, B. Bayle, M. de Mathelin, and A. Gangi, "In vivo model estimation and haptic characterization of needle insertions," *Int. J. Robot. Res.*, vol. 26, no. 11–12, pp. 1283–1301, Nov. 2007.

[26] O. A. Shergold and N. A. Fleck, "Experimental investigation into the deep penetration of soft solids by sharp and blunt punches, with application to the piercing of skin," *J. Biomech. Eng.*, vol. 127, no. 5, pp. 838–848, Oct. 2005.

[27] H. Kataoka, T. Washio, K. Chinzei, K. Mizuhara, C. Simone, and A. M. Okamura, "Measurement of the tip and friction force acting on a needle during penetration," in *Proc. 5th Int. Conf. Med. Image Comput. Comput.-Assisted Intervention*, 2002, pp. 216–223.

[28] T. Washio and K. Chinzei, "Needle force sensor, robust and sensitive detection of the instant of needle puncture," in *Proc. 7th Int. Conf. Med. Image Comput. Comput.-Assisted Intervention*, 2004, pp. 113–120.

[29] D. De Lorenzo, Y. Koseki, E. De Momi, K. Chinzei, and A. Okamura, "Experimental evaluation of a coaxial needle insertion assistant with enhanced force feedback," in *Proc. 33rd Annu. Int. Conf. IEEE Eng. Med. Biol. Soc.*, 2011, pp. 3447–3450.

[30] Y. Koseki, D. De Lorenzo, K. Chinzei, and A. M. Okamura, "Coaxial needle insertion assistant for epidural puncture," in *Proc. IEEE/RSJ Int. Conf. Intell. Robots Syst.*, Sep. 2011, pp. 2584–2589.

[31] K. J. Kuchenbecker, J. G. Park, and G. Niemeyer, "Characterizing the human wrist for improved haptic interaction," in *Proc. ASME Int. Mech. Eng. Congr. Expo., Symp. Adv. Robot Dyn. Control*, 2003, vol. 2, pp. 519–528.

[32] I. Sack, B. Beierbach, J. Wuerfel, D. Klatt, U. Hamhaber, S. Papazoglou, P. Martus, and J. Braun, "The impact of aging and gender on brain viscoelasticity," *Neuroimage*, vol. 46, no. 3, pp. 652–657, Jul. 2009.

[33] K. L. Monson, W. Goldsmith, N. M. Barbaro, and G. T. Manley, "Significance of source and size in the mechanical response of human cerebral blood vessels," *J. Biomech.*, vol. 38, no. 4, pp. 737–744, Apr. 2005.

[34] S. Misra, K. T. Ramesh, and A. M. Okamura, "Modeling of tool-tissue interactions for computer-based surgical simulation: A literature review," *Presence Teleoperators Virtual Environ.*, vol. 17, no. 5, pp. 463–491, Oct. 2008.

[35] L. Frasson, T. Parittotokkaporn, A. Schneider, B. L. Davies, J. F. V. Vincent, S. E. Huq, P. Degenaar, and F. M. R. Baena, "Biologically inspired microtexturing: Investigation into the surface topography of next-generation neurosurgical probes," in *Proc. 30th Annu. Int. Conf. IEEE Eng. Med. Biol. Soc.*, Aug. 2008, pp. 5611–5614.

[36] A. Wittek, T. Dutta-Roy, Z. Taylor, A. Horton, T. Washio, K. Chinzei, and K. Miller, "Subject-specific non-linear biomechanical model of needle insertion into brain," *Comput. Methods Biomech. Biomed. Eng.*, vol. 11, no. 2, pp. 135–146, Apr. 2008.

Danilo De Lorenzo received the B.Sc. and M.Sc. degrees in biomedical engineering from the Politecnico di Milano, Milan, Italy, in 2005 and 2008, respectively, and the Ph.D. degree in biomedical and biomechanical engineering from the joint program between the three Italian Technical Universities (Politecnico di Milano, Torino, and Bari) in 2012.

He has been a Ph.D. visiting student at the Technion Institute of Technology, Haifa, Israel, and at The Johns Hopkins University, Baltimore, MD. He is currently a Research Fellow at the Politecnico di Milano. His scientific interests include medical robotics, computer-assisted surgery, haptics, soft-tissue mimicking materials and modeling, and biomedical ultrasound signal processing.

Yoshihiko Koseki received the Master of Science degree in precision machinery engineering from the University of Tokyo, Tokyo, Japan, in 1996.

From 1996 to 2001, he was a Researcher in Mechanical Engineering Laboratory, Tokyo, Japan. Since 2001, he has been a Researcher at the National Institute of Advanced Industrial Science and Technology, Tsukuba, Japan. From 2010 to 2011, he was a Visiting Scholar at the Johns Hopkins University, Baltimore, MD. His current research interests include the field of medical robotics, especially MRI-compatible robotics. He is also interested in parallel mechanism and its application to medical robotics.

Elena De Momi was born in Legnago, Italy, on March 19, 1978. She received the M.Sc. degree in biomedical engineering and the Ph.D. degree in bioengineering from the Politecnico di Milano, Milan, Italy, in 2002 and 2006, respectively

She is currently an Assistant Professor at the Politecnico di Milano. She spent several months at the University of Bern, Berne, Switzerland, and at Carnegie Mellon University, Pittsburgh, PA. Since 2006, she has been involved in research on medical images registration, navigation systems for surgery, and surgical robotics. She is the Project Manager of the ACTIVE project (FP7-ICT-270460) for robotic neurosurgery and the local Principal Investigator of the EUROSURGE CA (FP7-ICT-288233). His scientific activities are documented by publications in international journals and by a national patent.

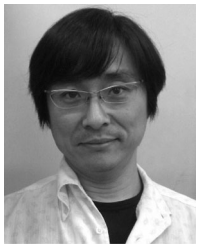

Kiyoyuki Chinzei (M'06) received the Ph.D. degree in medical machinery engineering from the University of Tokyo, Tokyo, Japan, in 1993.

He started the Surgical Assist Technology Group, National Institute of Advanced Industrial Science and Technology, Tsukuba, Japan. His main research interests include surgical robotics and image-guided therapy, as well as the safety and regulatory affair of such technology. He serves as a National Expert of ISO/IEC TC62/SC62A JWG9 (safety of medical devices using robotic technology).

Allison M. Okamura (S'98–A'00–M'03–SM'09–F'11) received the B.S. degree from the University of California, Berkeley, in 1994, and the M.S. and Ph.D. degrees from Stanford University, Stanford, CA, in 1996 and 2000, respectively, all in mechanical engineering.

She is currently an Associate Professor of mechanical engineering at Stanford University. Her research interests include haptics, teleoperation, robot-assisted surgery, tissue modeling and simulation, rehabilitation robotics, and prosthetics.

Dr. Okamura received the 2004 National Science Foundation CAREER Award, the 2005 IEEE Robotics and Automation Society Early Academic Career Award, and the 2009 IEEE Technical Committee on Haptics Early Career Award. She is an Associate Editor of the IEEE TRANSACTIONS ON HAPTICS.